Neural Comput & Applic (2018) 30:2129–2144
https://doi.org/10.1007/s00521-016-2739-0

ORIGINAL ARTICLE

Engineering strength of fiber-reinforced soil estimated by swarm intelligence optimized regression system

Jui-Sheng Chou[1] · **Ngoc-Tri Ngo**[1,2]

Received: 27 December 2015 / Accepted: 23 November 2016 / Published online: 28 December 2016

Abstract Fiber-reinforced soil (FRS) has been used as a promising alternative material for civil and construction engineering. Shear strength of FRS is influenced complexly by many factors including fiber properties, soil properties, and stress conditions. This inherent complexity limits the ability of designers to assess shear strength parameters and has made it difficult to establish a mathematical model for accurately predicting the FRS shear strength. Accurately estimating the shear strength of FRS is vital for civil engineers in designing geotechnical structures and management. Thus, this work proposed a novel computational method, namely a swarm intelligence optimized regression (SIOR) system to estimate the peak shear strength of randomly distributed FRS. The SIOR system integrates a machine learning technique with an enhanced swarm intelligence algorithm to obtain reliable and good performance in prediction process. The real-world FRS dataset collected over the past 30 years was used to validate the proposed system. To demonstrate the capability of the proposed system, the SIOR modeling results were compared with those obtained using numeric predictive models. The analytical results confirm that the SIOR system is superior to a baseline machine learning model and empirical methods via cross-fold validation and hypothesis test with accuracy improvement from 44.7 to 99.7% in mean absolute percentage error. Therefore, the SIOR system can significantly improve the prediction accuracy and facilitate civil engineers in estimating the shear strength of the FRS.

Keywords Artificial intelligence · Swarm intelligence optimization · Machine learning · Fiber-reinforced soil · Composite materials · Civil and construction engineering · Shear strength · Prediction

1 Introduction

Fiber-reinforced soil (FRS) has been applied in civil engineering ecosystems for many years. The FRS is a promising alternative material for localized repair of slopes and reinforcement of thin soil veneers where planar reinforcement is difficult to implement due to geometric constraints [1]. However, estimating the FRS behaviors has confirmed a difficult task because shear strength of FRS is influenced complexly by many factors including fiber characteristics, soil properties, and stress conditions. Accurately estimating the shear strength of FRS is vital for civil engineers in designing geotechnical structures and management.

Some researchers have proposed methods to estimate the peak shear strength of FRS. Particularly, a statistical technique [2], a discrete formulation [3], and energy dissipation formulations [4] have been developed for predicting FRS shear strength. Although these conventional methods are convenient, their accuracy is limited because simplified models do not adequately consider complex mechanisms of soil–fiber interaction [5]. Relationship among shear strength of FRS and fiber characteristics, soil

✉ Jui-Sheng Chou
jschou@mail.ntust.edu.tw

Ngoc-Tri Ngo
D10205804@mail.ntust.edu.tw; trinn@dut.udn.vn

[1] Department of Civil and Construction Engineering, National Taiwan University of Science and Technology, Taipei, Taiwan

[2] Faculty of Project Management, University of Science and Technology, The University of Danang, Da Nang, Vietnam

properties, and stress conditions is inherently nonlinear. This inherent complexity limits the ability of designers to assess shear strength parameters and has made it difficult to establish a mathematical model for accurately predicting the FRS shear strength.

Because of the importance of improving the prediction performance, machine learning (ML)-based methods have been developed to enhance prediction accuracy and efficiency [6, 7]. ML-based approaches have confirmed the potential solutions for solving real-world engineering problems [8–11]. Literature shows that no study has used ML-based method to estimate shear strength of FRS in geotechnical systems. Therefore, the ML-based approaches are potential techniques for shear strength prediction of FRS.

Among the ML techniques, the least squares support vector regression (LSSVR) method proposed by Suykens et al. [12] is one of the prevailing AI methods. The LSSVR greatly reduces computation complexity and increases efficiency compared to standard SVR. It has been widely used in civil engineering field [13–15]. Most studies agree that the predictive accuracy of a SVR-based model is superior to that of other ML-based models [16–18]. The performance of the LSSVR model depends highly on its hyperparameters, namely the regularization parameter (C) and radial basis function kernel parameter (σ). For improving the prediction ability, appropriately selecting the LSSVR hyperparameters is a challenging optimization problem.

Swarm intelligence (SI) has attracted great interest and attention [19, 20]. Examples of SI-based algorithms include artificial bee colony, particle swarm optimization, cuckoo search, and firefly algorithm (FA). The FA is a particularly efficient SI-based algorithm because it has two major advantages over the others: automatic subdivision and the ability to handle multimodality [21]. SI-based algorithms have been successful in solving a wide range of problems in various domains [22]. As a part of this work, an enhanced nature-inspired metaheuristic algorithm was used to dynamically optimize the LSSVR hyperparameters.

In this regard, this study proposes a new computational method, namely a swarm intelligence optimized regression (SIOR) system to estimate the peak shear strength of randomly distributed fiber-reinforced soil. The system integrates an LSSVR and an enhanced SI optimization algorithm, namely smart firefly algorithm (SFA), in which the SFA is used to fine-tune the LSSVR hyperparameters.

As the original scientific contribution, the proposed SIOR system provides a new method of estimating the FRS shear strength in the geotechnical system which is efficient and reliable. In addition, the new SFA algorithm is integrated into the SIOR system, which can efficiently optimize the LSSVR hyperparameters; consequently, the prediction accuracy of the SIOR system is significantly improved. In particular, a user-friendly interface of the SIOR system provides convenience to the users. Finally, a comparison analysis of the prediction performance between the proposed SIOR system, the baseline LSSVR, and empirical methods has been done via cross-fold validation and hypothesis test.

The proposed SIOR system was developed in MATLAB®. To demonstrate its efficacy, FRS dataset collected from 20 studies published during 1983–2015 was used to validate the system. Prediction performance was evaluated in terms of linear correlation coefficient (R), root-mean-square error (RMSE), mean absolute error (MAE), and mean absolute percentage error (MAPE).

The remainder of this paper is organized as follows. Section 2 reviews the relevant literature and empirical methods for calculating shear strength of FRS. The proposed system and evaluation theory are presented in Sect. 3. Section 4 discusses the data collection process, the system evaluation, and analytical results. The last section presents the concluding remarks.

2 Literature review

The FRS was used to strengthen the shear-resistant capacity of the geotechnical systems [23], reduce potential slope failure [24], improve soil rigidity and brittleness [25], repair slope veneer, and patch uneven surfaces, and serve as a more durable alternative to geogrid and geotextile [5]. Many prior researches confirmed the effectiveness of fiber reinforcement [26, 27]. The FRS has shown the effectiveness for repairing failed slopes where the irregular shape of soil patches limits the use of textile reinforcements and stabilizing subgrade in road construction [28].

Accurately predicting the peak friction angle of randomly distributed FRS is essential for efficient engineering design. In the past three decades, studies of FRS behavior [1, 3, 4, 26, 29–31] have included Zornberg, who introduced a discrete model for designing FRS slopes. Fibers are treated as discrete elements that contribute to stability by mobilizing tensile stresses along shear planes. Zornberg [3] applied the bilinear shear strength envelope, in which the fiber-induced distributed tension acting along a failure surface is added to the soil shear strength.

Michalowski and Čermák [4] further proposed an energy dissipation model for estimating the ultimate shear strength of randomly distributed FRS in the "fiber slip" confinement ranges. Similarly, Sadek et al. [32] proposed a mathematical model for predicting shear strength of fiber-reinforced sands. Sivakumar Babu et al. [27] examined

soil–fiber interaction in FRS by using numerical analysis to capture the overall stress–strain response. Recent studies indicate that peak friction angle of FRS is influenced by several factors, including soil properties, fiber characteristics, and stress conditions.

Instead of numerical modeling, Maher and Gray [30] performed triaxial compression tests to study the effects of soil properties, fiber characteristics, and other variables on sand reinforced with randomly distributed fibers. Ranjan et al. [2] performed triaxial compression tests on soil reinforced with randomly distributed fibers to identify the relationship between the shear strength of reinforced soil and fiber parameters, soil properties, and confining stress. In particular, Ahmad et al. [26] performed a series of triaxial tests to study the effect of oil palm empty fruit bunch (OPEFB) fiber on the shear strength of soil under drained and undrained triaxial test conditions. According to their experimental results, addition of OPEFB fiber significantly increases the peak shear strength of silty sand soil.

Li and Zornberg [1] performed triaxial compression tests and fiber pullout tests to evaluate how fiber tension is mobilized at varying shear strain levels. The experimental results confirmed that (1) full mobilization of fiber-induced tension requires comparatively high strain levels; (2) the initial density of the soil does not significantly affect the shear strength of FRS prepared with comparatively high fiber contents; (3) for FRS prepared with comparatively low fiber content and for conditions where the unreinforced soil stress–strain response shows a post-peak shear strength loss, the discrete framework should be applied when using the peak shear strength of the unreinforced soil to predict the equivalent shear strength of FRS.

Commonly used synthetic fibers include polypropylene (PP), polyethylene terephthalate, polyvinyl alcohol, glass, nylon, and steel. The advantages of these fibers include their high strength, high durability, easily controllable quality and yield, chemical resistance, and climate resistance. However, their disadvantage is their high environmental impact. Since synthetic fibers are resistant to biodecomposition and chemical corrosion, they prevent soil shrinkage and are resistant to weather and chemical changes. The most common of the above fibers is PP fiber [24]. Al-Refeai [33] indicated that PP fiber was superior to glass fiber and that the optimal length for fiber reinforcement was approximately 76 mm.

Several researchers have proposed empirical formulas for calculating the engineering strength of FRS. For example, Michalowski and Zhao [34] presented a mathematical formula as shown in Eq. (1) to estimate the shear-resistant strength of FRS.

$$\phi_f = 2\tan^{-1}\sqrt{\frac{X_f\eta_f M\tan\phi_w + 6K_p}{6 - X_f\eta_f M\tan\phi_w}} - \frac{\pi}{2} \tag{1}$$

where $M = K_p\sin\theta_0$, $K_p = \tan^2(45+\theta/2)$, $\theta_0 = \tan^{-1}\sqrt{K_p/2}$, η_f is fiber aspect ratio, ϕ is friction angle of soil, ϕ_w is interfacing friction angle between the sand and fiber, and X_f is fiber content (volume percentage).

Alternatively, Zornberg [3] developed a discrete model for predicting shear strength of FRS. Equation (2) is the mathematical formula of the discrete model.

$$\phi_f = \tan^{-1}((1+\alpha\cdot\eta_f\cdot X_f\cdot c_{i,\phi})\cdot\tan\phi) \tag{2}$$

where α is empirical coefficient, $\alpha \le 1$, ϕ is friction angle of soil, η_f is fiber aspect ratio, X_f is fiber content (volume percentage), $c_{i,\phi}$ is interface friction coefficient of soil ($\tan\phi_w/\tan\phi$), ϕ_w is interfacing friction angle between sand and fiber.

Although these empirical methods are convenient for designers, the accuracy of the estimated values is low because these empirical methods explore a limited number of factors and because the relationship between FRS strength parameter and predictive factors is highly nonlinear. Therefore, this study developed the novel computational method for improving accuracy in predicting the shear strength property of FRS. Particularly, this study enhances the optimization algorithm and LSSVR to provide high accuracy in facilitating FRS shear strength design.

3 Methodology

3.1 Least squares support vector regression

The LSSVR proposed by Suykens et al. [12] is a well-developed ML technique with many advanced features that enable good generalization capacity and fast computation. The LSSVR training process uses a least squares cost function to obtain a linear set of equations in the dual space so as to minimize computational cost. Accordingly, iterative methods, such as conjugate gradient efficiently solving a set of linear equations, are used to derive a solution. To reduce the computational burden of the LSSVR for function estimation, the regression model in this study used a quadratic loss function [35]. In a function estimation of the LSSVR, given a training dataset $\{x_k, y_k\}_{k=1}^N$, the classic linear LSSVR model related inputs X's with the output Y by minimizing the objective function which is formulated as Eq. (3).

$$\min_{\omega,b,e} J(\omega,e) = \frac{1}{2}\|\omega\|^2 + \frac{1}{2}C\sum_{k=1}^{N} e_k^2;$$
$$\text{subject to } y_k = \langle\omega,\varphi(x_k)\rangle + b + e_k, \quad k = 1,\ldots,N \tag{3}$$

where $J(\omega, e)$ is the optimization function; ω is the parameter of the linear approximator; $e_k \in R$ is error variables; $C \geq 0$ is a regularization constant that specifies the constant representing the trade-off between the empirical error and the flatness of the function; x_k is input patterns; y_k is prediction labels; and N is the sample size.

Since this is a typical optimization problem of a differentiable function with constraints, it can be solved by using Lagrange multipliers (α_k). The resulting LSSVR model for function estimation can be expressed as Eq. (4).

$$f(x) = \sum_{k=1}^{N} \alpha_k K(x, x_k) + b \tag{4}$$

where α_k, b are Lagrange multipliers and the bias term, respectively, and $K(x, x_k)$ is kernel function. In the feature space, the kernel function can be described as Eq. (5):

$$K(x, x_k) = \sum_{k=1}^{m} g_k(x) g_k(x_k) \tag{5}$$

In this study, the radial basis function (RBF) kernel was used not only because it has lower mathematical complexity compared to the polynomial kernel, but also because it effectively solves highly nonlinear problems. Equation (6) is the mathematical expression of the RBF kernel.

$$K(x, x_k) = \exp(-\|x - x_k\|^2 / 2\sigma^2) \tag{6}$$

where σ is the RBF width.

However, the prediction accuracy of the LSSVR is highly dependent on the determination of its hyperparameters. Therefore, as a part of this study, the enhanced SI algorithm was developed to optimize LSSVR hyperparameters, i.e., the regularization parameter (C) and the sigma of the RBF kernel (σ).

3.2 Enhanced swarm intelligence optimization algorithm

An enhanced SI optimization algorithm, i.e., SFA, is developed by combining the conventional FA and metaheuristic components, which are used to fine-tuning the conventional FA parameters.

3.2.1 Swarm intelligence-based algorithm

The computational intelligence has received great interest and attention in the literature. In the communities of optimization, computational intelligence, and computer science, bio-inspired algorithms, especially those SI-based algorithms are now become very popular [19, 36, 37]. The FA developed by Yang [38] is a stochastic, SI algorithm that efficiently finds the global optima of an optimization problem. The FA applies three idealized rules: (1) Each firefly is attracted to other fireflies regardless of gender because all fireflies are unisex; (2) the attractiveness of a firefly is proportional to its brightness and decreases as distance increases; additionally, a firefly moves randomly if no other firefly is brighter; and (3) the brightness of a firefly is affected or determined by the search space of the objective function.

For a maximization problem, the brightness value is simply set to be proportional to the value of the objective function. As the attractiveness of a firefly is proportional to the intensity of light that is visible to adjacent fireflies, the attractiveness β of a firefly satisfies Eq. (7).

$$\beta = \beta_0 e^{-\gamma r^2} \tag{7}$$

where β is the attractiveness of the firefly; β_0 is the attractiveness of the firefly at $r = 0$; r is the distance between the firefly of interest and any other, e is a constant coefficient, and γ is the absorption coefficient.

The distance between any two fireflies i and j at x_i and x_j, respectively, is the Cartesian distance, given by Eq. (8).

$$r_{ij} = \|x_i - x_j\| = \sqrt{\sum_{k=1}^{d} (x_{i,k} - x_{j,k})^2} \tag{8}$$

where r_{ij} is the distance between any two fireflies i and j at x_i and x_j, respectively; $x_{i,k}$ is the kth component of spatial coordinate x_i of the ith firefly; $x_{j,k}$ is the kth component of spatial coordinate x_j of the jth firefly, and d is the number of dimensions of the search space.

Equation (9) specifies the movement of the ith firefly when attracted to the more attractive (brighter) jth firefly.

$$x_i^{t+1} = x_i^t + \beta_0 e^{-\gamma r_{ij}^2}\left(x_j^t - x_i^t\right) + \alpha^t(\text{rand} - 0.5) \tag{9}$$

where x_i^{t+1} is the coordinate of the ith firefly in the $(t + 1)$th iteration; x_i^t is the coordinate of the ith firefly in the tth iteration; x_j^t is the coordinate of the jth firefly in the tth iteration; γ is the absorption coefficient and was set to explore global optima. The best result obtained in the sensitivity analysis of γ is $\gamma = 1$; $\beta_0 = \beta_{\min}$ is the attractiveness at $r_{ij} = 0$; α^t is a randomization parameter; rand is a random-number generator uniformly distributed within [0, 1].

The FA procedure can be summarized as follows. First, the initial firefly positions are randomly generated. Second, a given fitness function is used to evaluate each firefly. Third, fireflies move by using Eq. (9) in which fireflies with worse fitness values move toward fireflies with better fitness values. For the firefly with the best fitness value, the second part of Eq. (9) becomes zero. Therefore, its movement is randomly proportional to the coefficient α^t. The above procedure continues until a given number of iterations are reached.

Although FA is highly efficient in many applications, it often becomes trapped in a local optimum [39]. Moreover, setting tuning parameters that improve the convergence of the FA is challenging. The FA control parameters should be optimized for effectively balancing exploitation and exploration. Specifically, the balance between the exploration and exploitation capability of the conventional FA can be improved by enhancing the diversity of initial population of the FA, tuning attractiveness, adjusting randomization, and controlling movement of the FA.

3.2.2 Metaheuristic components in fine-tuning of swarm intelligence algorithm

The conventional FA uses three standard elements to perform an automatic search that proceeds toward global optimality: initial population, the attractiveness parameter, and the movement. These three terms are adjusted by the following metaheuristic components: chaotic maps, adaptive inertia weight (AIW), and Lévy flight. First, the logistic chaotic map and the Gauss/mouse chaotic map provide a highly diverse initial population and tune an attractiveness parameter in the FA implementation, respectively. Second, AIW is dynamically adjusted in the optimization process to control the local exploitation and the global exploration capabilities of the FA. Third, Lévy flight speeds up the local search by generating new optimal neighborhoods around the obtained best solution.

3.2.2.1 Logistic chaotic map for enhancing initial solution The FA uses a typical random approach to generate an initial solution. The two major disadvantages of this approach are its slow convergence and its tendency to become trapped in local optima because of reduced population diversity. For improving initial solution diversity and the quality of the initial population, logistic chaotic map is used to generate a highly diverse of fireflies in the initial stage. Equation (10) is the logistic map formula.

$$X_{n+1} = \eta X_n(1 - X_n) \tag{10}$$

where n denotes the number label of the individual firefly and X_n is the chaotic value for the nth firefly.

Since Eq. (10) is clearly deterministic, it exhibits chaotic dynamics when $\eta = 4.0$ and $X_0 \notin \{0.0, 0.25, 0.5, 0.75, 1.0\}$. It exhibits strong dependence on initial conditions and describes travel with ergodicity, irregularity and pseudorandomness. A minute difference in the initial values of populations can cause a considerable difference in its long-term behavior [40]. Thus, in all experiments in this work, initial firefly positions are generated using the logistic map equation, and parameter η was set to 4.0.

3.2.2.2 Gauss/mouse chaotic map for tuning attractiveness The Gauss/mouse map is the best way to tune the attractiveness parameter (β) of the FA [41]. Equation (11) describes the Gauss/mouse map used in this study instead of random parameters used in the conventional FA.

The Gauss/mouse map:

$$\beta_{chaos}^{t+1} = \begin{cases} 0 & \beta_{\text{chaos}}^{t} = 0 \\ 1/\beta_{chaos}^{t} \bmod (1) & \text{otherwise} \end{cases} \tag{11}$$

Eq. (7) is then updated to

$$\beta = (\beta_{chaos}^{t} - \beta_0)e^{-\gamma r_{ij}^2} + \beta_0 \tag{12}$$

3.2.2.3 Adaptive inertia weight for adjusting randomization The swarm-based algorithm can be improved by reducing the randomness of its parameters as the iteration proceeds. In the early stages of the search process, a high inertia weight can boost global exploration (in searches of new areas). However, in the late stages, the adaptive inertia weight, which is reduced in each stage, can improve the local exploitation of the optimal solution (finely tuning the current search area). Inertia weight accelerates convergence to the optimal solution and reduces the execution time of the simulation. The adaptive inertial weight controls the local exploitation and global exploration capabilities of the swarm algorithm.

The above issue is addressed by using a monotonically decreasing function of the inertia weight to change the randomization parameter α in the conventional FA. Since the adaptive inertia weight was used to adjust the randomization parameter α, the distances between fireflies are reduced to maintain the α within a reasonable range [Eq. (13)].

$$\alpha^t = \alpha_0\theta^t \tag{13}$$

where α_0 is the initial randomization parameter; α^t is the randomization parameter at tth iteration; θ is the randomness reduction constant ($0 < \theta < 1$); and t is the number of iterations. The selected value of θ is 0.9 in this implementation based on several trials and experiments, and $t \in [0, t_{\max}]$, where $t_{\max}$ is the maximum number of iterations.

3.2.2.4 Lévy flights for controlling movement Random walk theory plays a critical role in modern swarm intelligence and evolutionary optimization algorithms. Lévy flights are a random walk in which the step length is a Lévy distribution. The step lengths have no characteristic scale, i.e., the second moment or even the first moment may diverge, and the distribution exhibits self-affine properties. The steps form a random walk process with a power-law step-length distribution with a heavy tail.

Fig. 1 Pseudocode for the enhanced swarm intelligence optimization algorithm

Begin
Perform objective function f(x), x = (x1, ..., xd)^T
Set the search space and the number of generation
Generate initial population of fireflies xi (i = 1, 2, ..., n) using ***logistic chaotic map***
Determine light intensity Ii at xi by f(xi)
Define light absorption coefficient
Generate initial population, k = 0
while (*t* ≤MaxGeneration) **do**
(1) Update the generation number, k = k +1
(2) Tune randomization parameter α by using ***adaptive inertia weight*** *(* $\alpha = \alpha_0 \cdot 0.9^t$ *)*
(3) Tune attractiveness parameter β by using ***Gauss/mouse chaotic map***
for *i* = 1: no. fireflies
for *j* = 1: no. fireflies
if (*Ij* > *Ii*)
Move firefly i toward j in d-dimension by ***Lévy flight****;*
end if
*Vary attractiveness with distance r via exp[-γ*r]*
Evaluate new solutions and update light intensity
end for *j*
end for *i*
Rank the fireflies and find the current best
end while
Obtain and visualize post-process results
End

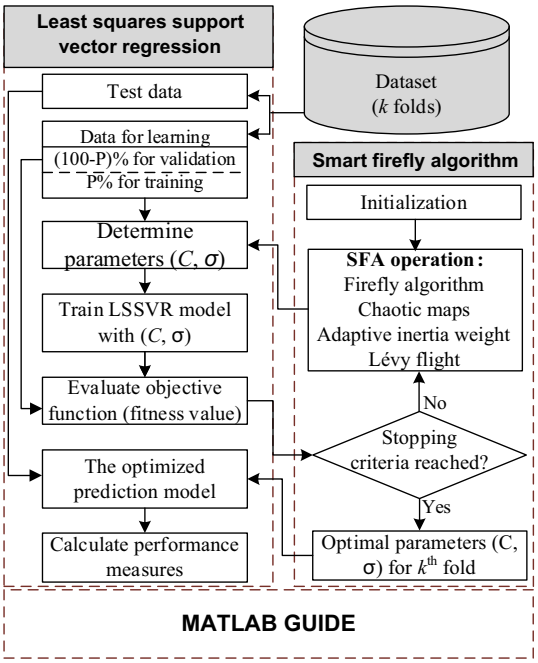

Fig. 2 Flowchart of system building and evaluation process

Lévy flights are defined such that each jump, regardless of size, takes one unit of time [42]. Lévy flights are used to generate random numbers in two steps: random selection of a direction and generation of steps that obey the selected Lévy distribution. In this work, directions were generated with uniform distributions. The Mantegna algorithm, which is the most efficient, is used to generate steps from a symmetric Lévy stable distribution. The step length s in the Mantegna algorithm is calculated using Eq. (14).

$$\text{Lévy} \sim s = \frac{u}{|v|^{1/\tau}} \tag{14}$$

where u and v are drawn from normal distributions, as follows:

$$u \sim N\left(0, \sigma_u^2\right), \quad v \sim N\left(0, \sigma_v^2\right) \tag{15}$$

$$\sigma_u = \left\{ \frac{\Gamma(1+\tau)\sin(\pi\tau/2)}{\Gamma[(1+\tau)/2]\tau 2^{(\tau-1)/2}} \right\}^{1/\tau}, \quad \sigma_v = 1 \tag{16}$$

where $\Gamma(z)$ is the Gamma function

$$\Gamma(z) = \int_0^\infty t^{z-1} e^{-t} \mathrm{d}t \tag{17}$$

A Lévy walk speeds up the local search by generating new solutions around the best solution obtained so far. This behavior is applicable for optimizing the search in optimization problems, and preliminary results verify the promise of so doing [43]. Therefore, Eq. (9) is revised to Eq. (18).

$$x_i^{t+1} = x_i^t + \beta(x_j^t - x_i^t) + \alpha^t \text{sign}[\text{rand} - 0.5] \otimes \text{Lévy} \tag{18}$$

where the second term is the attraction; the attractiveness parameter (β) is updated by Eq. (12); the third term denotes the randomization that is associated with the Lévy flights [Eqs. (14)–(17)]; and α^t is the randomization parameter [Eq. (13)]. The product operator $\otimes$ indicates entry-wise

Fig. 3 Pseudocode for the swarm intelligence optimized regression model

1. Initialization stage
Subdivide the data into *k* subsets as *learning data (training data and validation data)* and *test data*
Initialize search parameters *via* chaotic map operator (logistic map)
Set the *initial population, the number of generations in each stage, and the boundary of optimized parameters*.
2. Perform *k* folds such that, for each fold, the following steps are performed
while (t < MaxIterations) **do**
2.1 Perform optimization procedure *via* SFA
(1) AlphaNew \\ $\alpha = \alpha_0 * 0.9^t$ (Adaptive inertia weight)
(2) BetaNew \\ Vary β *via* chaotic map operator (Gauss/mouse map)
(3) Evaluate SFA \\ Call *f(m)* from step 2.2
(4) SortSFA \\ Sort fitness values and go to step 2.3
(5) MoveSFA \\ Random component has altered by Lévy flight
end while
2.2 SFA-LSSVR function validation
Set the kernel (*rbf*) and loss-function (*least-square*) parameters
Train model with hyperparameters (C, σ)
Evaluate the trained (optimized) LSSVR model using validation data
Determine the fitness function $f(C, \sigma)$ and go to step 2.1 (4)
2.3 Have the stopping criteria been met?
If the criteria have been met, go to step 3.
Otherwise, go to step 2.1 (5).
3. Optimized LSSVR model
Incorporate the identified kernel parameters into the model learning
Calculate the average accuracy over the *k* test folds
4. Plot stage
Evaluate the post-process results and visualize the results
Confirm the best solution

multiplication. The term sign[rand − 0.5] with rand ∈ [0, 1] denotes a random sign or direction when the random step length is drawn from a Lévy distribution. Figure 1 presents the pseudocode of the enhanced swarm intelligence optimization algorithm.

3.3 Swarm intelligence optimized regression system

This study developed the SIOR system that integrates LSSVR with the enhanced swarm intelligence optimization algorithm (i.e., SFA). The SIOR system is used to predict the peak shear strength (peak friction angle) of composite FRS, in which the SFA is used to fine-tune the LSSVR hyperparameters (i.e., C and σ). For ensuring the generalization capacity of the proposed regression system, 10-fold cross-validation algorithm as recommended in the literature [44] was used in this study.

Specifically, the dataset was randomly divided into mutually exclusive 10 folds. Of these, 9 were used for model learning, and the tenth fold was used for model testing. This procedure was repeated 10 times with a rotary fold as test data. Each time, $P\%$ $(0 < P < 100)$ of learning data (training data) was used to train the SIOR system, $(100 - P)\%$ of learning data (validation data) was used to validate the optimal LSSVR hyperparameters. Notably, the P value can be customized by trial experiments for a particular dataset and is usually set as 60–90 for most cases. Test data were then used to evaluate the learning performance of the LSSVR model after optimization. Figure 2 is a flowchart of the process used to build and evaluate the proposed SIOR system.

The objective function of the SFA is derived from the RMSE value of validation data. Equation (19) describes the fitness function of the SFA.

$$\text{The objective function: } f(C,\sigma) = \text{RMSE}^{\text{Optimization}}_{Validation-data} = \sqrt{\frac{1}{n_v}\sum_{i=1}^{n_v}(y' - y)^2} \tag{19}$$

$$\text{Search space: } C_{\min} \le C \le C_{\max} \text{ and } \sigma_{\min} \le \sigma \le \sigma_{\max}$$

$$\text{Maximum iteration: } t_{\max}$$

where $f(C, \sigma)$ is the fitness functions of the SFA optimization algorithm; $\text{RMSE}^{\text{Optimization}}_{Validation-data}$ is the root-mean-square error calculated according to the predicted (y') and actual (y) values based on the validation data; n_v is the sample size of validation data; $C_{\min}$, $C_{\max}$, σ_{min}, $\sigma_{\max}$, and $t_{\max}$ are user-defined constants based on a series of trial experiments.

Figure 3 presents the pseudocodes for the SIOR model. The firefly search parameters are initialized via a logistic chaotic map operator [Eq. (10)]. The inside loop of the firefly search process is performed as follows: (1) to dedicate the "AlphaNew" function, modify the initial value of

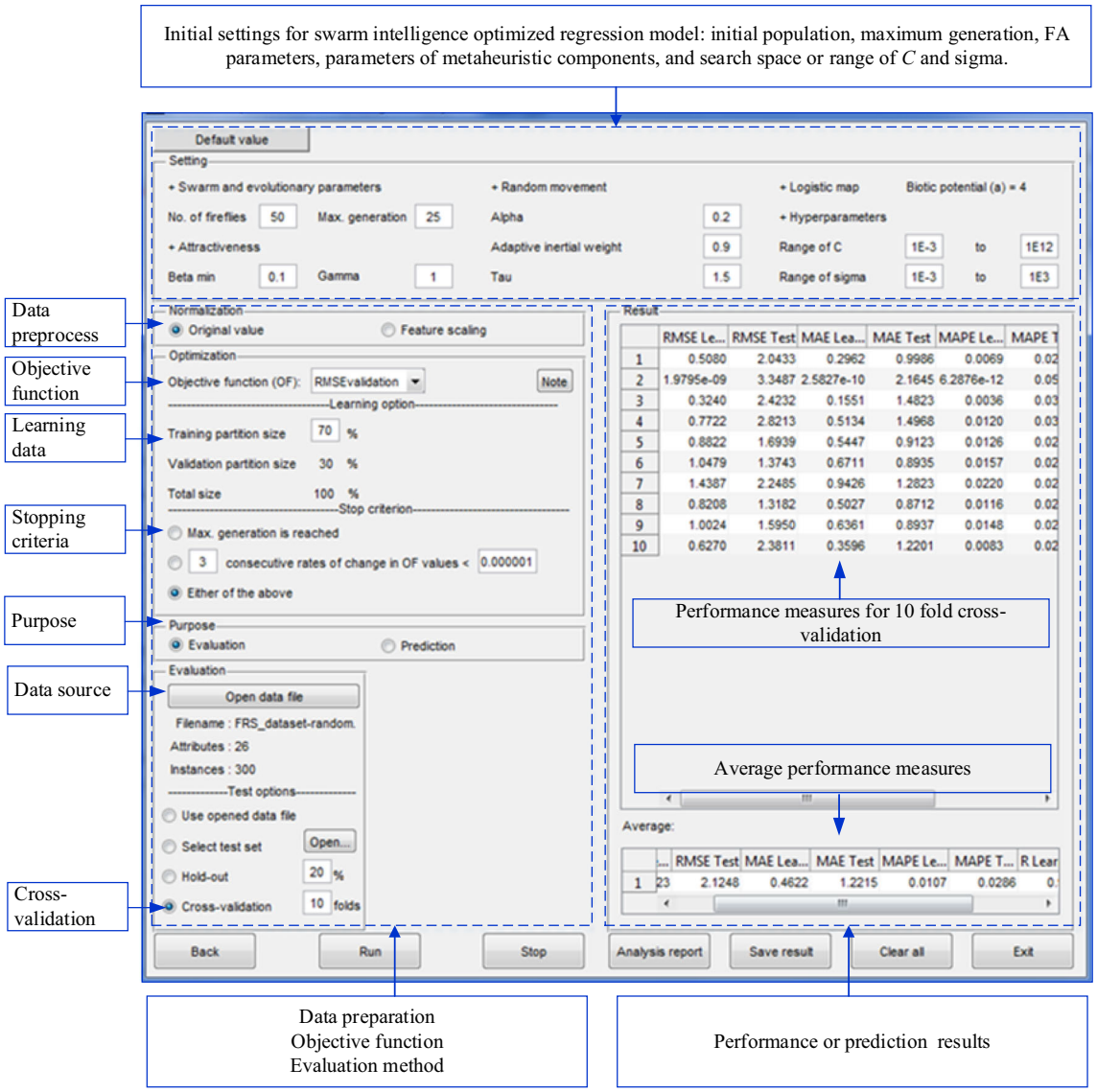

Fig. 4 SIOR system interface

parameter α by multiplying it by 0.9^t (adaptive inertia weight) [Eq. (13)]; (2) use the Gauss/mouse chaotic map to compute the "BetaNew" function [Eq. (12)]; (3) use the "EvaluateSFA" algorithm to evaluate LSSVR solution quality via the fitness function $f(C, \sigma)$ [Eq. (19)]; (4) use the "SortSFA" function to select the individual with the best fitness in the population; finally, (5) use "MoveSFA" to move the firefly toward more attractive individuals via Lévy flight in the search space [Eq. (18)].

The proposed SIOR system was implemented in MATLAB environment, and MATLAB GUIDE was used to design a user-friendly interface. Figure 4 illustrates the operating procedure with the system interface built in the MATLAB GUIDE environment. The SIOR system interface has three main parts: (1) initial parameter settings for the swarm intelligence optimized regression model; (2) data preparation, selection of objective function, and option of evaluation method; and (3) performance or prediction results. The initial parameter settings can be set to default values, or they can be customized by users. In the SIOR system, each firefly represents a possible solution, and its light intensity is inversely proportional to its objective function value. After the stopping criteria are reached, the best solution is defined as the firefly with the highest light intensity.

3.4 Evaluation theory

3.4.1 Performance measures

The prediction accuracy of the proposed system was evaluated in terms of R, RMSE, MAE, and MAPE. Table 1

Table 1 Mathematical formulas for performance measures

Measure	Formula
Linear correlation coefficient (R)	$R = \frac{n_d \sum y \cdot y' - (\sum y)(\sum y')}{\sqrt{n_d(\sum y^2) - (\sum y)^2}\sqrt{n_d(\sum y'^2) - (\sum y')^2}}$
Mean absolute percentage error (MAPE)	$\text{MAPE} = \frac{1}{n_d}\sum_{i=1}^{n_d}\left\|\frac{y-y'}{y}\right\|$
Mean absolute error (MAE)	$\text{MAE} = \frac{1}{n_d}\sum_{i=1}^{n_d}\|y - y'\|$
Root-mean-square error (RMSE)	$\text{RMSE} = \sqrt{\frac{1}{n_d}\sum_{i=1}^{n_d}(y' - y)^2}$

y' = predicted value; y = actual value; and n_d = number of data samples

summarizes the calculation formulas for these indexes. The R is a common measure of the fit of the curve to the actual data. The RMSE is computed to find the square error of the prediction compared to actual values and to find the square root of the summation value. That is, the RMSE is the average distance of a data point from the fitted line measured along a vertical line. This tool efficiently identifies undesirably large differences. The MAE is a measure of the difference between a forecasted value and the actual value. It computes the average magnitude of errors between predicted and actual values, disregarding direction of errors. The MAPE is a statistical measure of the performance of predictive models. Because it gives relative values, it is unaffected by the size or unit of actual and predicted values for fairly comparing models.

3.4.2 Cross-fold validation method

Predictive performance is often validated by using a k-fold cross-validation algorithm to minimize bias associated with randomly sampled training and test data. Since cross validation randomly assigns individual cases into distinct folds, the folds themselves are often stratified. In stratified k-fold cross validation, the proportions of predictor labels (responses) in the folds approximate those in the original dataset. Since 10 folds are considered optimal [44], 10-fold cross validation was used to justify the predictive consistency of the model. The performance of the proposed model is measured in terms of average R, RMSE, MAE, and MAPE.

4 System evaluation

4.1 Data collection and descriptive statistics

The experimental data for the 300 valid samples were collected from 20 FRS-related studies published during 1983–2015 [1, 4, 25–27, 30, 32–34, 45–55]. The shear strength of FRS is affected by many factors, including fiber characteristics, soil properties, and stress conditions. These factors have been conducted by various researchers in the above 20 literatures. Since these factors have been validated in several studies, they were used to predict FRS shear strength.

The complete dataset was divided into two parts, using the cross-validation algorithm: a learning dataset containing 270 samples and a test dataset containing the remaining data (30 samples). The 70% of learning dataset (189 samples) serving as training data was used to train the SIOR system. The remainder of learning dataset (81 samples) serving as validation data was used to determine the optimal LSSVR hyperparameters C and σ. After optimal hyperparameters were identified by the SFA, test data were then used to evaluate the learning performance of the LSSVR.

Table 2 describes the statistical attributes of the dataset. The predictor variables are fiber type (X_1), fiber length (X_2), fiber diameter (X_3), fiber content—volume percentage (X_4), fiber content—weight percentage (X_5), fiber gravity (X_6), soil type (X_7), soil grade (X_8), soil D50 (X_9), soil friction angle (X_{10}), cohesion (X_{11}), unit weight of dry soil (X_{12}), soil interface coefficient (X_{13}), fiber–soil interface friction angle (X_{14}), confining pressure/normal stress (X_{15}). Fiber types (X_1) in the dataset included nine types: polypropylene or polyprop (PP), polyamide, steel, glass, reed, coir, palm, polyester (PET), and unreinforced. Soil types (X_7) include fine sand, medium sand, medium dune, medium mortar, and coarse sand. Soil grade (X_8) consists of SP (poorly graded sand) and SW (well-graded sand) according the Unified Soil Classification System (USCS). The response is FRS friction angle (Y).

4.2 Analytical results and discussion

As discussed above, obtaining accurate solution for the shear strength of FRS requires optimization of the LSSVR hyperparameters, including the regularization parameter

Table 2 Statistical parameters for fiber-reinforced soil dataset

Attribute	Symbol	Type	Unit	Min	Average	Max
Fiber type	X_1	Category	n/a	–	–	–
Fiber length, L_f	X_2	Numeric	mm	6.000	27.344	51.000
Fiber diameter, D_f	X_3	Numeric	mm	0.010	0.301	1.250
Fiber content–volume percentage, X_f	X_4	Numeric	%	0.170	1.014	5.530
Fiber content–weight percentage, χ_m	X_5	Numeric	%	0.100	1.095	6.549
Fiber gravity	X_6	Numeric	–	0.580	1.610	7.850
Soil type	X_7	Category	n/a	–	–	–
Soil grade	X_8	Category	n/a	–	–	–
Soil D50	X_9	Numeric	mm	0.090	0.409	1.450
Soil friction angle, ϕ	X_{10}	Numeric	°	26.400	34.400	43.000
Cohesion (c')	X_{11}	Numeric	kPa	0.000	0.178	6.900
Unit weight of dry soil	X_{12}	Numeric	kN/m^3	12.998	15.621	18.394
Soil interface coefficient ($c_{i,\phi}$)	X_{13}	Numeric	–	0.370	0.765	1.326
Fiber–soil interface friction angle (ϕ_w)	X_{14}	Numeric	°	16.000	24.019	40.000
Confining pressure or normal stress, σ_3' or σ_n	X_{15}	Numeric	kPa	20.000	174.970	600.000
FRS friction angle ϕ_f	Y	Numeric	°	31.700	40.409	67.400

Fiber types (X_1) include polypropylene or polyprop (PP), polyamide, steel, glass, reed, coir, palm, polyester (PET), and unreinforced. Soil types (X_7) include fine sand, medium sand, medium dune, medium mortar, and coarse sand. Soil types (X_8) consist of SP (poorly graded sand) and SW (well-graded sand)

Table 3 Parameter settings for the enhanced swarm intelligence optimization algorithm

Parameter	Purpose	Setting
No. of fireflies	Population size	50
Max generation	Stopping criteria	25
Logistic chaotic map	Generate initial population with high diversity	Random generation based on Eq. (10), biotic potential η is set to 4
$\beta_{\min}$	Minimum value of attractiveness parameter β	0.1
γ	Absorption coefficient	1
Gauss/mouse chaotic map	Automatically tune β parameter	Random generation based on Eq. (12)
α	Randomness of firefly movement	$\alpha_o = 0.2$
Adaptive inertia weight	Control the swarm algorithm's local and global exploration capabilities	$\theta = 0.9$
Lévy flight	Speed up the local search by generating new solutions around the best solution	$\tau = 1.5$

(C) and sigma (σ) of the RBF kernel. Consequently, this is a two-dimensional optimization problem. In this study, the SFA was served as a search engine to optimize the C and σ.

Table 3 shows the setting for the SFA parameters during the optimization process. Particularly, the values of C and σ are set to large ranges of [0.001, 10^{12}] and [0.001, 10^3], respectively. Population size of the SFA (i.e., the number of LSSVR hyperparameter pairs, C and σ) is set 50. The optimal hyperparameters of the LSSVR are obtained when the stopping criteria are reached, which is set as maximum iteration of 25 or consecutive rates of change in the objective function values less than 0.000001.

Table 4 presents the optimal values of LSSVR hyperparameters, including C and σ for 10 folds of the dataset.

Table 4 Optimal values for least squares support vector regression hyperparameters

Fold No.	Regularization parameter (C)	Sigma parameter (σ)
1	2.114e+4	204.2528
2	1.796e+4	66.8431
3	1.027e+5	924.7595
4	1.059e+4	74.3376
5	9.811e+5	1000.0000
6	1.805e+4	4.1334
7	2.018e+4	213.2658
8	8.534e+4	1000.0000
9	10e+6	952.5887
10	455.8886	47.8604

The results show that for predicting the peak shear strength of FRS, SFA optimizes the ranges of C and σ as [445.8886, 10e+6] and [4.1334, 10e+3], respectively, in the cross-fold validation procedure.

Table 5 shows the performance measures obtained by the proposed SIOR system during the learning and test phases. The SIOR system had average R, RMSE, MAE, and MAPE values of 0.958, 2.125°, 1.222°, and 2.86%, respectively, for the FRS test data, which demonstrated the effectiveness of the system. Notably, in the cross-fold validation procedure, the best MAPE value obtained by the proposed system was 2.01% at fold 8, and the best R value was 0.986 at fold 6.

Figure 5 displays the observed (actual) and predicted peak friction angles of FRS with their performance measures in test data for 10 folds. The linear correlation patterns demonstrated the good prediction performance for the peak shear strength property of randomly distributed FRS.

The performance of the proposed system is also compared with that of the baseline LSSVR and widely used empirical methods proposed by Zornberg [3] and Michalowski and Zhao [34]. Moreover, Najjar et al. [5] suggested that the empirical methods are unsuitable when confining pressure is higher than 400 kPa or aspect ratio of fibers is larger than 200 which is a very thin fiber. Thus, FRS samples with the above properties were excluded from the dataset when using empirical methods to calculate FRS shear strength.

All inputs shown in Table 2 are used in comparison with the proposed SIOR system and the baseline LSSVR (namely group 1). To fairly compare performance between the proposed system and the empirical method proposed by Michalowski and Zhao [34], the considered inputs are fiber aspect ratio η_f (L_f/D_f), soil friction angle ϕ, fiber–soil interface friction angle ϕ_w, and fiber content–volume percentage X_f (namely group 2). Likewise, to compare performance between the SIOR system and the empirical method proposed by Zornberg [3], the inputs are soil friction angle ϕ, fiber aspect ratio η_f, fiber content–volume percentage X_f, soil interface coefficient $c_{i,\phi}$, and fiber–soil interface friction angle ϕ_w (namely group 3).

Table 5 Performance measures obtained by the SIOR system

Fold No.	Learning data				Test data			
	R	RMSE (°)	MAE (°)	MAPE (%)	R	RMSE (°)	MAE (°)	MAPE (%)
1	0.998	0.508	0.296	0.69	0.977	2.043	0.999	2.36
2	1.000	0.000	0.000	0.00	0.906	3.349	2.164	5.22
3	0.999	0.324	0.155	0.36	0.940	2.423	1.482	3.57
4	0.995	0.772	0.513	1.20	0.912	2.821	1.497	3.29
5	0.993	0.882	0.545	1.26	0.982	1.694	0.912	2.19
6	0.991	1.048	0.671	1.57	0.986	1.374	0.893	2.16
7	0.983	1.439	0.943	2.20	0.953	2.249	1.282	2.92
8	0.994	0.821	0.503	1.16	0.985	1.318	0.871	2.01
9	0.991	1.002	0.636	1.48	0.982	1.595	0.894	2.04
10	0.997	0.627	0.360	0.83	0.956	2.381	1.220	2.83
Min	0.983	0.000	0.000	0.00	0.906	1.318	0.871	2.01
Average	0.994	0.742	0.462	1.07	0.958	2.125	1.222	2.86
Max	1.000	1.439	0.943	2.20	0.986	3.349	2.164	5.22
SD	0.005	0.404	0.271	0.632	0.030	0.653	0.411	0.994

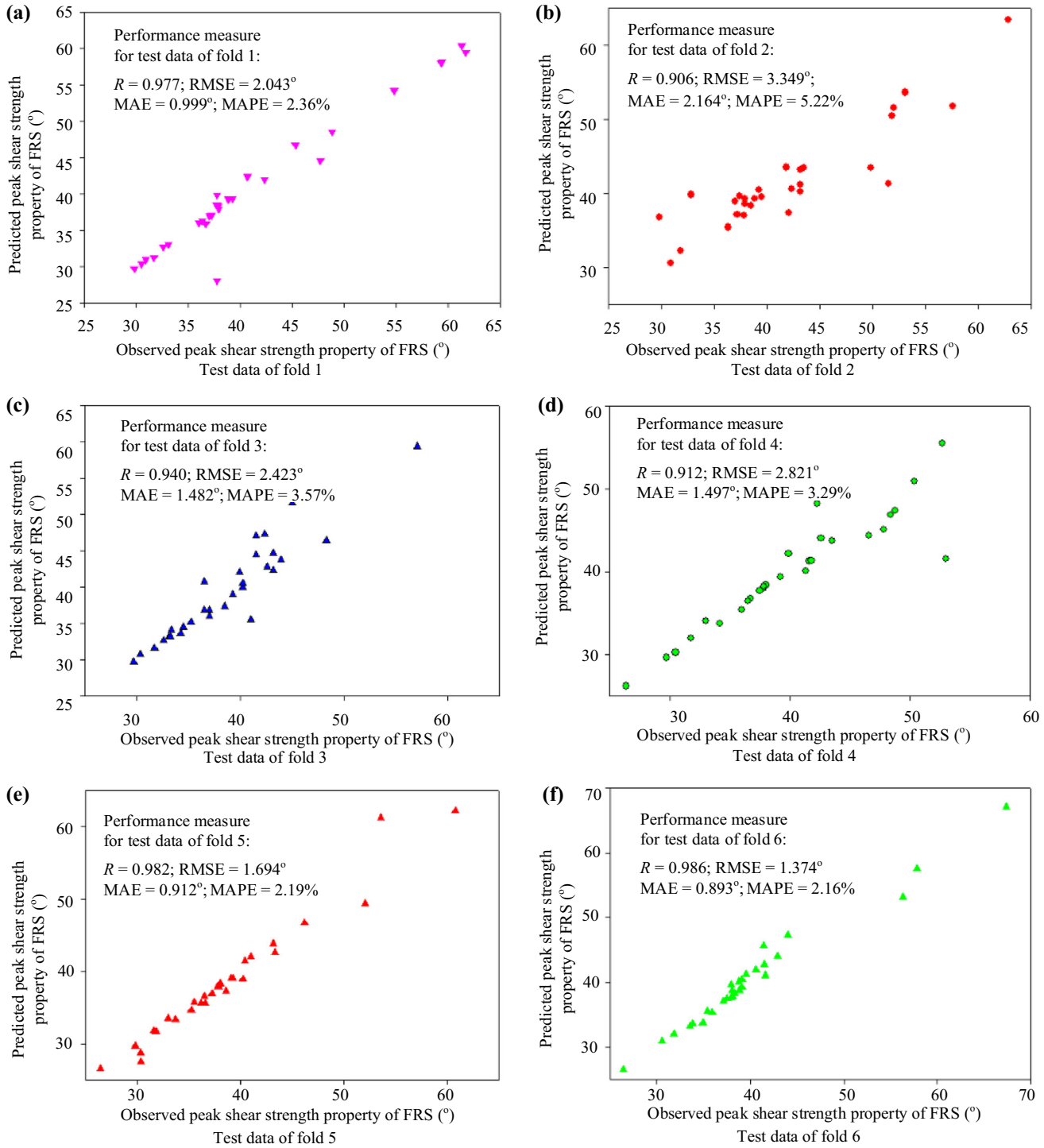

Fig. 5 Observed and predicted peak friction angles of FRS in test data for 10 folds

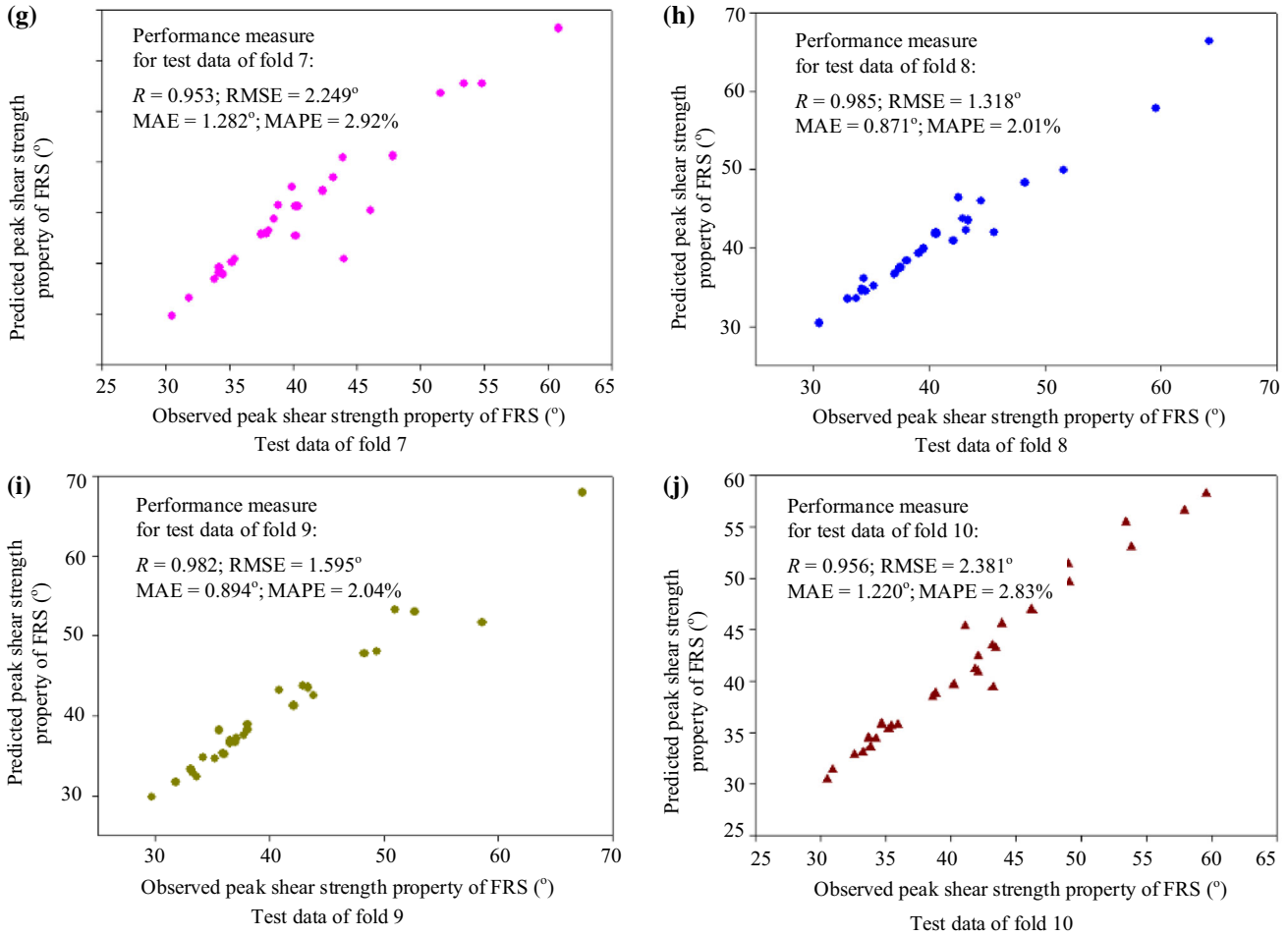

Fig. 5 continued

Table 6 Performance measures for the proposed system, the baseline model, and methods reported in the literature

Model/method	Performance measure				Improvement (%)			
	R	RMSE (°)	MAE (°)	MAPE (%)	*R*	RMSE	MAE	MAPE
Group 1—considered 15 inputs								
Baseline LSSVR	0.716	5.759	4.129	10.19				
SIOR system (15 inputs)	0.958	2.125	1.222	2.86	33.8*	63.1*	70.4*	71.9*
Group 2—considered 5 inputs (X_2, X_3, X_4, X_{10}, X_{14})								
Michalowski and Zhao [34]	0.660	7.450	5.220	10.60				
SIOR system (5 inputs)	0.888	3.539	1.630	3.62	34.5*	52.5*	68.8*	99.7*
Group 3—considered 5 inputs (X_2, X_3, X_4, X_{10}, X_{13})								
Zornberg [3], $\alpha = 1$	0.790	5.480	4.240	9.80				
SIOR system (5 inputs)	0.852	4.440	1.507	5.42	7.8**	19.0**	64.5*	44.7*

Measurements of performance improvements and hypothesis testing results are calculated using average performance measures

*, ** Significant levels higher than 1 and 5%, respectively

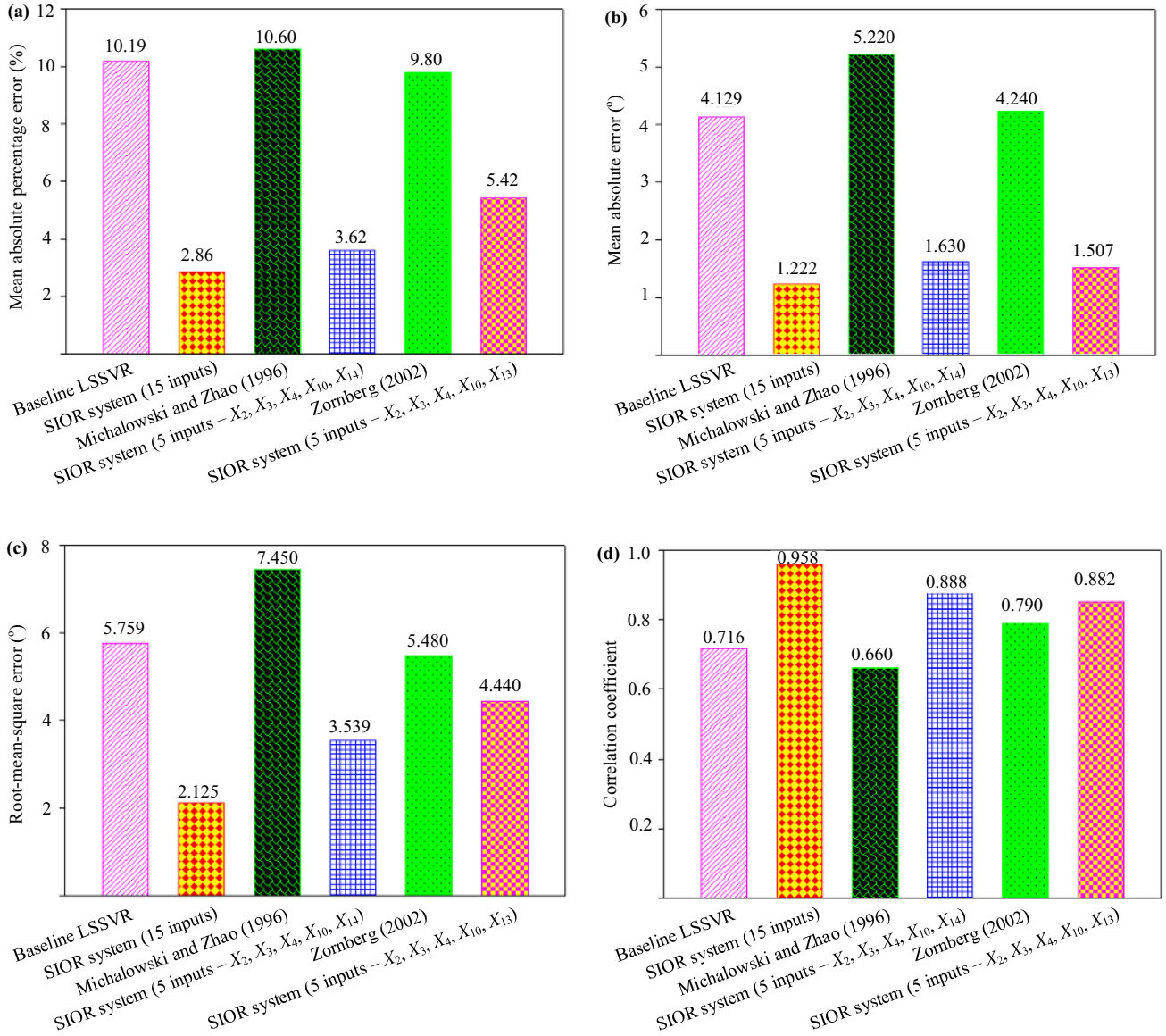

Fig. 6 Prediction performance comparisons between the proposed system and the others

For the three above groups, Table 6 shows the performance evaluation results obtained by the proposed system and those obtained by other methods. Figure 6 depicts the prediction accuracy of the methods. The comparison results for group 1 confirmed that performance of the SIOR system is better than that of the baseline LSSVR in terms of all performance indexes. The accuracy of predictions of peak shear strength of FRS obtained by the SIOR system is significantly improved and reaches 33.8%, 63.1%, 70.4%, and 71.9% in *R*, RMSE, MAE, and MAPE, respectively.

Similarly, compared with the empirical methods used in group 2 and group 3, the numerical results indicate that the proposed SIOR system outperformed the methods proposed by previous studies [3, 34]. Particularly, the proposed system improved *R*, RMSE, MAE, and MAPE by 34.5/7.8%, 52.5/19.0%, 68.8/64.5%, and 99.7/44.7%, respectively, with the significant level higher than 1 or 5% (Table 6). Therefore, the hypothesis tests confirmed that the accurate and reliable prediction of shear strength of FRS by the SIOR system was superior to those of other predictive methods.

5 Conclusions

Fiber-reinforced soil is a promising alternative material for civil engineering systems. Shear strength of FRS is influenced complexly by many factors including fiber characteristics, soil properties, and stress conditions. Accurately estimating the shear strength of FRS is vital for civil

engineers in designing geotechnical structures and management. Thus, this study developed a SIOR system in MATLAB environment to predict the peak shear strength friction angle of randomly distributed FRS.

This study makes three main contributions: Metaheuristic components are used to improve the efficacy of the conventional swarm algorithm; the enhanced algorithm effectively optimizes LSSVR hyperparameters. Thus, accuracy in predicting FRS shear strength can be improved. The proposed system was established by integrating the LSSVR and the advanced swarm intelligence optimization algorithm to assist civil engineers in designing optimally FRS.

A cross-fold validation method was then used to justify its generalization capability. In experiments performed using FRS data collected from 20 studies published during the 1983–2015, the results for the learning and test stages suggested that the system is efficient for forecasting the shear strength of randomly distributed FRS. The SIOR system also simplifies analyses of how the shear strength of FRS is affected by each mechanical and geometric characteristic of soils and fibers.

Compared with the baseline LSSVR and previous empirical methods, the proposed system yielded more convincing results. Particularly, *R*, RMSE, MAE, and MAPE improvements were 33.8%, 63.1%, 70.4%, and 71.9%, respectively, in comparison with the baseline LSSVR. The system achieves MAPEs of 5.42% and 3.62%, and improves prediction accuracy by 44.7% and 99.7% compared to the conventional empirical methods [3, 34]. The SIOR system is a potentially superior alternative for predicting FRS shear strength property. Therefore, civil engineers can use the novel system to achieve accurate and reliable prediction of shear strength in randomly distributed FRS.

References

1. Li C, Zornberg J (2013) Mobilization of reinforcement forces in fiber-reinforced soil. J Geotech Geoenviron Eng 139(1):107–115. doi:10.1061/(ASCE)GT.1943-5606.0000745
2. Ranjan G, Vasan RM, Charan HD (1996) Probabilistic analysis of randomly distributed fiber-reinforced soil. J Geotech Eng 122(6):419–426. doi:10.1061/(ASCE)0733-9410(1996)122:6(419)
3. Zornberg JG (2002) Discrete framework for limit equilibrium analysis of fibre-reinforced soil. Géotechnique 52:593–604
4. Michalowski R, Čermák J (2003) Triaxial compression of sand reinforced with fibers. J Geotech Geoenviron Eng 129(2):125–136. doi:10.1061/(ASCE)1090-0241(2003)129:2(125)
5. Najjar S, Sadek S, Alcovero A (2013) Quantification of model uncertainty in shear strength predictions for fiber-reinforced sand. J Geotech Geoenviron Eng 139(1):116–133. doi:10.1061/(ASCE)GT.1943-5606.0000742
6. Chou J-S, Cheng M-Y, Wu Y-W (2013) Improving classification accuracy of project dispute resolution using hybrid artificial intelligence and support vector machine models. Expert Syst Appl 40(6):2263–2274. doi:10.1016/j.eswa.2012.10.036
7. X-h T, W-h B, X-l H, Wang W (2011) Reliability analysis using radial basis function networks and support vector machines. Comput Geotech 38(2):178–186. doi:10.1016/j.compgeo.2010.11.002
8. Chou J-S, Lin C (2013) Predicting disputes in public-private partnership projects: classification and ensemble models. J Comput Civ Eng 27(1):51–60. doi:10.1061/(ASCE)CP.1943-5487.0000197
9. Chou J-S, Pham A-D (2013) Enhanced artificial intelligence for ensemble approach to predicting high performance concrete compressive strength. Constr Build Mater 49:554–563. doi:10.1016/j.conbuildmat.2013.08.078
10. Wei X-K, Li Y-H, Li Y-F, Zhang D-F (2008) Enclosing machine learning: concepts and algorithms. Neural Comput Appl 17(3):237–243
11. Cao MS, Pan LX, Gao YF, Novák D, Ding ZC, Lehký D, Li XL (2015) Neural network ensemble-based parameter sensitivity analysis in civil engineering systems. Neural Comput Appl. doi:10.1007/s00521-015-2132-4
12. Suykens JAK, Gestel TV, Brabanter JD, Moor BD, Vandewalle J (2002) Least squares support vector machines. World Scientific, Singapore
13. Zhang H, Yang F, Li Y, Li H (2015) Predicting profitability of listed construction companies based on principal component analysis and support vector machine—evidence from China. Autom Constr 53:22–28. doi:10.1016/j.autcon.2015.03.001
14. Chou J-S, Chong WK, Bui D-K (2016) Nature-inspired metaheuristic regression system: programming and implementation for civil engineering applications. J Comput Civ Eng 30(5):04016007. doi:10.1061/(ASCE)CP.1943-5487.0000561
15. Chou J-S, Ngo N-T (2016) Time series analytics using sliding window metaheuristic optimization-based machine learning system for identifying building energy consumption patterns. Appl Energy 177:751–770. doi:10.1016/j.apenergy.2016.05.074
16. Pal M, Deswal S (2011) Support vector regression based shear strength modelling of deep beams. Comput Struct 89(13–14):1430–1439. doi:10.1016/j.compstruc.2011.03.005
17. Martins FF, Begonha A, Amália Sequeira Braga M (2012) Prediction of the mechanical behavior of the Oporto granite using data mining techniques. Expert Syst Appl 39(10):8778–8783. doi:10.1016/j.eswa.2012.02.003
18. Chou J-S, Ngo N-T, Chong WK (2016) The use of artificial intelligence combiners for modeling steel pitting risk and corrosion rate. Eng Appl Artif Intell. doi:10.1016/j.engappai.2016.09.008
19. Yang X-S (2014) Analysis of algorithms. In: Nature-inspired optimization algorithms. Elsevier, Oxford, pp 23–44. doi:10.1016/B978-0-12-416743-8.00002-6
20. Roque CMC, Martins PALS (2015) Differential evolution for optimization of functionally graded beams. Compos Struct 133:1191–1197. doi:10.1016/j.compstruct.2015.08.041
21. Yang X-S (2014) Firefly algorithms. In: Yang X-S (ed) Nature-inspired optimization algorithms. Elsevier, Oxford, pp 111–127. doi:10.1016/B978-0-12-416743-8.00008-7
22. Chou J-S, Ngo N-T, Pham A-D (2016) Shear strength prediction in reinforced concrete deep beams using nature-inspired metaheuristic support vector regression. J Comput Civ Eng 30(1):04015002. doi:10.1061/(ASCE)CP.1943-5487.0000466
23. Ibraim E, Fourmont S (2007) Behaviour of sand reinforced with fibres. Soil Stress Strain Behav Meas Model Anal 146:807–818. doi:10.1007/978-1-4020-6146-2_60
24. Hejazi SM, Sheikhzadeh M, Abtahi SM, Zadhoush A (2012) A simple review of soil reinforcement by using natural and

synthetic fibers. Constr Build Mater 30:100–116. doi:10.1016/j.conbuildmat.2011.11.045
25. Consoli N, Prietto P, Ulbrich L (1998) Influence of fiber and cement addition on behavior of sandy soil. J Geotech Geoenviron Eng 124(12):1211–1214. doi:10.1061/(ASCE)1090-0241(1998)124:12(1211)
26. Ahmad F, Bateni F, Azmi M (2010) Performance evaluation of silty sand reinforced with fibres. Geotext Geomembr 28(1):93–99. doi:10.1016/j.geotexmem.2009.09.017
27. Sivakumar Babu GL, Vasudevan AK, Haldar S (2008) Numerical simulation of fiber-reinforced sand behavior. Geotext Geomembr 26(2):181–188. doi:10.1016/j.geotexmem.2007.06.004
28. Chauhan MS, Mittal S, Mohanty B (2008) Performance evaluation of silty sand subgrade reinforced with fly ash and fibre. Geotext Geomembr 26(5):429–435. doi:10.1016/j.geotexmem.2008.02.001
29. Gray DH, Ohashi H (1983) Mechanics of fiber reinforcement in sand. J Geotech Eng 109(3):335–353. doi:10.1061/(ASCE)0733-9410(1983)109:3(335)
30. Maher M, Gray D (1990) Static response of sands reinforced with randomly distributed fibers. J Geotech Eng 116(11):1661–1677. doi:10.1061/(ASCE)0733-9410(1990)116:11(1661)
31. Cruz M, Santos JM, Cruz N (2015) Using neural networks and support vector regression to relate Marchetti dilatometer test parameters and maximum shear modulus. Appl Intell 42(1):135–146
32. Sadek S, Najjar S, Freiha F (2010) Shear strength of fiber-reinforced sands. J Geotech Geoenviron Eng 136(3):490–499. doi:10.1061/(ASCE)GT.1943-5606.0000235
33. Al-Refeai TO (1991) Behavior of granular soils reinforced with discrete randomly oriented inclusions. Geotext Geomembr 10(4):319–333. doi:10.1016/0266-1144(91)90009-L
34. Michalowski R, Zhao A (1996) Failure of fiber-reinforced granular soils. J Geotech Eng 122(3):226–234. doi:10.1061/(ASCE)0733-9410(1996)122:3(226)
35. Wang H, Hu D (2005) Comparison of SVM and LS-SVM for regression. In: International conference on neural networks and brain, 2005. ICNN&B '05, pp 279–283. doi:10.1109/ICNNB.2005.1614615
36. Tang D, Dong S, Cai X, Zhao J (2015) A two-stage quantum-behaved particle swarm optimization with skipping search rule and weight to solve continuous optimization problem. Neural Comput Appl. doi:10.1007/s00521-015-2014-9
37. Altun A, Şahman M (2013) Cost optimization of mixed feeds with the particle swarm optimization method. Neural Comput Appl 22(2):383–390. doi:10.1007/s00521-011-0701-8
38. Yang X-S (2008) Firefly algorithm. Nature-inspired metaheuristic algorithms. Luniver Press, Bristol
39. Fister I, Fister I Jr, Yang X-S, Brest J (2013) A comprehensive review of firefly algorithms. Swarm Evol Comput 13:34–46. doi:10.1016/j.swevo.2013.06.001
40. Liu B, Wang L, Jin Y-H, Tang F, Huang D-X (2005) Improved particle swarm optimization combined with chaos. Chaos Solitons Fractals 25(5):1261–1271. doi:10.1016/j.chaos.2004.11.095
41. He D, He C, Jiang LG, Zhu HW, Hu GR (2001) Chaotic characteristics of a one-dimensional iterative map with infinite collapses. IEEE Trans Circuits Syst I Fundam Theory Appl 48(7):900–906
42. Geisel T, Nierwetberg J, Zacherl A (1985) Accelerated diffusion in Josephson junctions and related chaotic systems. Phys Rev Lett 54(7):616–619
43. Pavlyukevich I (2007) Cooling down Lévy flights. J Phys A Math Theor 40(41):12299. doi:10.1088/1751-8113/40/41/003
44. Kohavi R (1995) A study of cross-validation and bootstrap for accuracy estimation and model selection. In: The international joint conference on artificial intelligence, pp 1137–1143
45. Gray D, Al-Refeai T (1986) Behavior of fabric-versus fiber-reinforced sand. J Geotech Eng 112(8):804–820. doi:10.1061/(ASCE)0733-9410(1986)112:8(804)
46. Shao W, Cetin B, Li Y, Li J, Li L (2014) Experimental investigation of mechanical properties of sands reinforced with discrete randomly distributed fiber. Geotech Geol Eng 32(4):901–910. doi:10.1007/s10706-014-9766-3
47. Ibraim E, Fourmont S (2007) Behaviour of sand reinforced with fibres. In: Ling H, Callisto L, Leshchinsky D, Koseki J (eds) Soil stress–strain behavior: measurement, modeling and analysis, vol 146., Solid mechanics and its applicationsSpringer, Berlin, pp 807–818. doi:10.1007/978-1-4020-6146-2_60
48. Yetimoglu T, Salbas O (2003) A study on shear strength of sands reinforced with randomly distributed discrete fibers. Geotext Geomembr 21(2):103–110. doi:10.1016/S0266-1144(03)00003-7
49. Consoli NC, Casagrande MDT, Coop MR (2007) Performance of a fibre-reinforced sand at large shear strains. Géotechnique 57:751–756
50. Consoli NC, Festugato L, Heineck KS (2009) Strain-hardening behaviour of fibre-reinforced sand in view of filament geometry. Geosynth Int 16:109–115
51. Nataraj MS, McManis KL (1997) Strength and deformation properties of soils reinforced with fibrillated fibers. Geosynth Int 4:65–79
52. Consoli NC, Montardo JP, Donato M, Prietto PD (2004) Effect of material properties on the behaviour of sand—cement—fibre composites. Proc ICE Ground Improv 8:77–90
53. Chen C-W (2007) A constitutive model for fiber-reinforced soils. University of Missouri, Columbia
54. Gregory GH (2006) Shear strength, creep and stability of fiber-reinforced soil slopes. Oklahoma State University, Stillwater
55. Al-Refeai T, Al-Suhaibani A (1998) Dynamic and static characterization of polypropylene fiber-reinforced dune sand. Geosynth Int 5(5):443–458